J Comput Neurosci
DOI 10.1007/s10827-011-0367-3

Detecting effective connectivity in networks of coupled neuronal oscillators

Erin R. Boykin · Pramod P. Khargonekar · Paul R. Carney · William O. Ogle · Sachin S. Talathi

Received: 1 February 2011 / Revised: 13 September 2011 / Accepted: 23 September 2011

Abstract The application of data-driven time series analysis techniques such as Granger causality, partial directed coherence and phase dynamics modeling to estimate effective connectivity in brain networks has recently gained significant prominence in the neuroscience community. While these techniques have been useful in determining causal interactions among different regions of brain networks, a thorough analysis of the comparative accuracy and robustness of these methods in identifying patterns of effective connectivity among brain networks is still lacking. In this paper, we systematically address this issue within the context of simple networks of coupled spiking neurons. Specifically, we develop a method to assess the ability of various effective connectivity measures to accurately determine the true effective connectivity of a given neuronal network. Our method is based on decision tree classifiers which are trained using several time series features that can be observed solely from experimentally recorded data. We show that the classifiers constructed in this work provide a general framework for determining whether a particular effective connectivity measure is likely to produce incorrect results when applied to a dataset.

Keywords Granger causality · Partial directed coherence · Phase dynamics modeling · Effective connectivity · Neuronal oscillators · Decision tree classifiers

Action Editor: Rob Kass

E. R. Boykin · P. P. Khargonekar
Department of Electrical and Computer Engineering, University of Florida, Gainesville, FL 32611, USA

E. R. Boykin
e-mail: erinrt@gmail.com

P. P. Khargonekar
e-mail: ppk@ece.ufl.edu

W. O. Ogle
J. Crayton Pruitt Family Department of Biomedical Engineering, University of Florida, Gainesville, FL 32611, USA
e-mail: wogle@bme.ufl.edu

P. R. Carney
Department of Pediatrics, Neurology, Neuroscience, and Biomedical Engineering, University of Florida, Gainesville, FL 32611, USA
e-mail: carnepr@peds.ufl.edu

S. S. Talathi (✉)
Department of Pediatrics, Neuroscience, and Biomedical Engineering, University of Florida, Gainesville, FL 32611, USA
e-mail: talathi@ufl.edu

1 Introduction

The importance of neuronal networks in coordinating brain function has been well-established in numerous studies. At the single-cell level, specialized circuits of neuronal oscillators have been implicated in memory formation, visual processing, learning, and a variety of other motor and cognitive tasks (Deister et al. 2009; Fries 2009; Buzsaki 2006; Buzsaki and Draguhn 2004). Of particular interest is the ability of neuronal networks to synchronize their firing activity, since this behavior has been linked to cognitive functions such as memory, attention and decision making (Uhlhaas and Singer 2010; Ward 2003) as well as pathological brain

Published online: 14 October 2011

states such as epilepsy (Uhlhaas and Singer 2010) and Parkinson's disease (Hammond et al. 2007). In order to understand how complex dynamical phenomenon such as synchronization emerge in neuronal networks, it is important to empirically characterize the connectivity structure of the network so as to determine how neurons in the network influence each other. Analysis of connectivity in neuronal networks is therefore of great importance both in fundamental neuroscience as well as clinical applications (Sporns 2010).

There are three related but distinct notions of connectivity: structural (anatomical), functional (dynamical) and effective (anatomical and dynamical). Structural connectivity refers to physical connections between neurons, functional connectivity refers to simple characterization of temporal correlations between spatially distinct neurons, and effective connectivity (EC) refers to the direct causal influence that one neuron or neuronal system exerts over the other (Friston 2002; Sporns 2010). As suggested above, for many neurological phenomena, understanding the EC between neurons is crucial. In particular, the ability to correctly infer EC from neural time series recordings is particularly important.

In recent years, a variety of techniques for EC analysis have been explored and used. In particular, data driven time series inference (TSI) techniques such as Granger causality (GC), partial directed coherence (PDC) and phase dynamic modeling (PDM) have been explored extensively and applied to many experimental neural data sets (Brovelli et al. 2004; Cadotte et al. 2010; Havlicek et al. 2010; Liao et al. 2010; Sato et al. 2009). These techniques are particularly appealing as they do not require a known anatomical model of the system under study. Several recent theoretical and computational studies (Winterhalder et al. 2005; Lungarella et al. 2007) have, however, shown that these TSI techniques can produce incorrect estimates for EC when the data being analyzed are highly synchronized (e.g., in epilectic networks). Although these limitations have been observed in theory, not much is known about the conditions (quantitative constraints) under which application of a given TSI technique on an experimental neuronal time series yields correct results. An upper bound on the level of synchronization that can be tolerated by PDC and PDM before they produce incorrect EC estimates has been recently provided in Smirnov et al. (2007). To the best of our knowledge, there still does not exist a usable methodology for delineating the conditions under which various TSI techniques yield correct EC analysis results.

Our long term objective is to develop a methodology that can help in assessing the accuracy of time-series based EC analysis techniques. In this paper we take the first steps in this direction. Here, we propose a methodology with two key steps: (1) computation of certain key features from the observed neuronal time series data and (2) a decision tree based classifier that uses these features as inputs and produces an indicator of validity of the given TSI technique on the data set under analysis. We develop our methodology on bivariate time series data generated from a simple network of two coupled Morris Lecar (ML) neuron models (Morris and Lecar 1981). The performance of the resulting two-node decision tree classifiers is then tested on an experimental data set comprising of a hybrid network of a model neuron dynamically coupled to a live neuron obtained from an adult male Sprague Dawley rat hippocampal brain slice. While, the extension of our proposed method to generic networks with greater than two nodes is beyond the scope of present work, here we present some practical suggestions on how two-node decision tree classifiers can be used to assess performance of TSI techniques in estimating EC in a network comprising of three or more nodes.

The simplest neuronal network with a well defined dynamic connectivity structure is a feed-forward network of two neuronal oscillators. We therefore use a simple unidirectional network of coupled Morris–Lecar (ML) neuronal oscillators as a template network for obtaining simulated datasets for classifier training. The choice of ML neuronal oscillators is motivated by the fact that the ML neuron model is a minimal conductance based biophysically realistic neuron model with the ability to generate pulse-like action potential events in response to synaptic perturbations (Morris and Lecar 1981; Izhikevich 2007). In particular, ML neurons are most suited to model real fast spiking neurons that respond with continuous action potentials to constant current stimulation. ML neurons have very large dynamic range and can fire at arbitrarily low frequencies and exhibit square-root current frequency relationship, which is very similar to those observed for fast spiking inhibitory neurons in the hippocampus (Lecar 2007). Although we have used ML neuron models and two neuron networks for decision tree training, in principle, the proposed *two step structure* can be used with other neuron models and neuronal networks with known connectivity structures. We extract the following three features from the neuronal time series data in order to develop our proposed decision tree classifier: (1) phase coherence, which is a metric for synchronization in the network, (2) coefficient of variation of interspike intervals, which is a metric for degree of noise in the network, and (3) difference in intrinsic firing frequencies, which is a metric for the overall excitability in the

network. The rationale for our choice of these features is further explained in Section 4.1.

For our study, we consider the following linear TSI methods: GC (Geweke 1982, 1984; Granger 1969), PDC (Baccala and Sameshima 2001) and a modified version of PDC known as generalized PDC (GPDC) (Winterhalder et al. 2005; Baccala et al. 2007). We also include PDM in our analysis since it is specifically designed for narrow-band interacting oscillators and can handle a moderate amount of nonlinearity in the data (Rosenblum and Pikovsky 2001).

We begin by considering two unidirectionally coupled ML neurons under three different coupling scenarios: (1) linear diffusive coupling, which models an electrical synapse or gap junction (Bennett 1997; Chow and Kopell 2000), (2) nonlinear, fast threshold modulation coupling, which models a fast time scale chemical synapse (Somers and Kopell 1993), and (3) nonlinear threshold coupling, which models a slow time scale chemical synapse (Abarbanel et al. 2003). For each coupling scheme, sample time series datasets are generated by varying the coupling strengths thereby controlling for the level of synchrony in the network, the noise levels, and intrinsic firing frequencies, which control the degree of dynamical activity within the network. The result is a large ensemble of time series datasets with known EC structure. For each network instance and the corresponding time series, we estimate the EC in the network using various TSI analysis techniques. Since we know the EC structure, we can then label whether a given TSI yields correct or incorrect EC result. Using these labels and features, we train decision tree classifiers. We have also investigated other machine learning techniques such as support vector machines. We ultimately chose decision tree classifiers since their accuracy is at least as good as other classifiers and, more importantly, they admit very appealing qualitative interpretations. We have tested our method on several simulated and an experimental neuronal time series datasets. The simulated datasets are from two and three neuron networks. The experimental network is a hybrid network constructed using the dynamic clamp set up and comprises of a live neuron coupled synaptically interacting with a computer neuron model via a computer model for synapse.

In summary, this work represents a novel paradigm for meta-analysis of TSI techniques for EC analysis. We believe that the proposed structure of time series feature computation followed by a machine learning style classifier can be used in other neuroscience applications. Since the EC structure is known in the simulation datasets, it is possible to train and test classifiers with EC structure known in advance. Such classifiers could be further validated using experimental datasets with known EC structures.

The rest of this paper is organized as follows. Section 2 describes the neuronal oscillator model and the networks used to generate sample datasets. Section 3 describes the mathematical details on the methods employed for estimating EC using GC, PDC, GPDC and PDM. Section 4 outlines the methodology for the construction of the classifiers. These classifiers are then used to assess the applicability of these methods for estimating the EC in the given network. Results are presented in Section 5 along with a discussion and conclusions in Section 6.

2 Neuron, synapse and network models

2.1 Neuron model

The ML model is described by the following equations:

$$C\frac{dv}{dt} = -g_{\mathrm{Ca}} m_\infty(v)(v - V_{\mathrm{Ca}}) - g_K w (v - V_K) - g_L (v - V_L) + I_{\mathrm{dc}} + I_{\mathrm{noise}} + I_{\mathrm{synapse}} \quad (1)$$

$$\frac{dw}{dt} = \lambda \frac{w_\infty(v) - w}{\tau_\infty(v)} \quad (2)$$

where

$$I_{\mathrm{noise}} = D\xi$$

$$I_{\mathrm{synapse}} = k f(v_{\mathrm{post}}, v_{\mathrm{pre}})$$

$$m_\infty(v) = 0.5\left[1 + \tanh\left(\frac{v - V_1}{V_2}\right)\right]$$

$$w_\infty(v) = 0.5\left[1 + \tanh\left(\frac{v - V_3}{V_4}\right)\right]$$

$$\tau_\infty(v) = \left[\cosh\left(\frac{v - V_3}{2V_4}\right)\right]^{-1}$$

Here v represents the transmembrane voltage of a neuron, w represents the action of the potassium current, I_{dc} is the external input current, I_{noise} is the input current due to noise and I_{synapse} is the input current from synaptically connected neurons. In the equation for I_{noise}, ξ is Gaussian white noise with zero mean, unit variance and D is the noise intensity. In the equation for I_{synapse}, k is the strength of coupling and the function, $f(v_{\mathrm{post}}, v_{\mathrm{pre}})$, represents the coupling type where v_{pre} is the membrane voltage of the presynaptic neuron and v_{post} is the membrane voltage of the postsynaptic neuron. This function is changed in order to model different realistic synapses, specifically linear diffusive coupling, fast threshold modulation

coupling, and nonlinear synaptic threshold coupling. The remaining parameters are set as follows: $V_1 = -1.2$ mV, $V_2 = 18$ mV, $V_3 = 12$ mV, $V_4 = 17.4$ mV, $V_L = -60$ mV, $V_K = -84$ mV, $V_{Ca} = 120$ mV, $g_L = 2$ μS/cm^2, $g_K = 8$ μS/cm^2, $g_{Ca} = 4$ μS/cm^2, $\lambda = \frac{1}{15}$ s^{-1}, and $C = 20$ μF/cm^2. For these parameters, the model exhibits Type I excitability, which means that oscillations can occur with arbitrarily low frequency as current is injected into the neuron (Ermentrout 1996).

2.2 Synapse models

The following three realistic synaptic coupling models are considered:

1. Linear diffusive coupling which models an electrical synapse or gap junction (Bennett 1997; Chow and Kopell 2000):

$$f(v_{post}, v_{pre}) = v_{pre} - v_{post} \tag{3}$$

2. Nonlinear, fast threshold modulation coupling which models a simplified chemical synapse (Somers and Kopell 1993):

$$f(v_{post}, v_{pre}) = 0.5\left[1 + \tanh\left(\frac{v_{pre} - V_{th}}{V_{slope}}\right)\right] \cdot (v_{post} - V_{rev}) \tag{4}$$

where $V_{th} = 0$ mV, $V_{slope} = 1$ mV and V_{rev} represents the synaptic potential, which is set to −84 mV to mimic the effect of inhibitory coupling.

3. Nonlinear, threshold coupling which models a chemical synapse and accounts for the dynamics of the release and absorption of neurotransmitters in the synaptic cleft (Abarbanel et al. 2003; Talathi et al. 2010):

$$f(v_{post}) = S(t)(v_{post} - V_{rev}))$$
$$\frac{dS}{dt} = \frac{S_\infty(v_{pre}(t) \cdot \theta(t)) - S(t)}{\tau[S_0 - S_\infty(v_{pre}(t) \cdot \theta(t))]} \tag{5}$$

where V_{rev} is defined as in Eq. (4). $\theta(t) = \sum_i \Theta(t - t_i) \cdot \Theta((t_i + \tau_R) - t)$ where $\Theta(\cdot)$ is the Heaviside step function and t_i is the time of the ith presynaptic neuronal spike. The timescale constant governing receptor binding is represented by τ and is set to 7.9 ms, $S_0 = 1.013$, and $\tau_R = \tau(S_0 - 1)$. Finally, S_∞ is the sigmoidal function defined as $S_\infty(v) = 0.5(1 + \tanh(120(v - 0.1)))$.

2.3 Network model

2.3.1 Simulated network

We consider simple networks composed of either two or three coupled ML neuronal oscillators in this work.

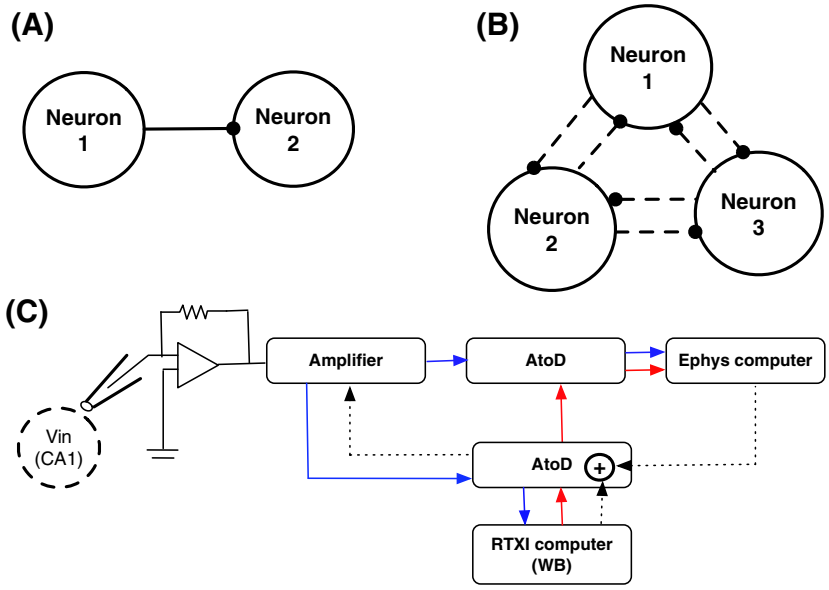

Fig. 1 The network structure of coupled neuronal oscillators considered in this work. (**a**) Neurons 1 and 2 are unidirectionally coupled with neuron 1 driving neuron 2. (**b**) Neurons 1–3 are randomly connected with dashed lines indicating possible coupling between neurons. (**c**) Dynamic clamp setup to generate hybrid network. *Blue arrow* shows the path for flow of live neuron membrane voltage (CA1 interneuron), the *red arrow* shows the path for flow of model neuron (WB interneuron) membrane voltage, the *dotted line* represents the flow of current into the live neuron; which is the sum of dc current bias to keep the neuron intrinsically firing and the synaptic current for unidirectional coupling from the model neuron to the live neuron

The first network is comprised of two unidirectionally coupled neuron models whose network structure is illustrated in Fig. 1(a). The second is an ensemble of 12 different 3-neuron networks, where networks are constructed by permuting the presence and absence of the various connections in Fig. 1(b).

2.3.2 Hybrid network

We also used a dynamic clamp setup to construct a hybrid network consisting of a living neuron coupled to a computer model neuron via nonlinear threshold coupling synapse model. The dynamic clamp provides an avenue for interfacing patch clamp recording techniques with computer generated neuron models to allow for real time interactions with a live neuron. Whole cell patch clamp recordings were obtained from interneurons in the stratum oriens of area CA1 of the hippocampus. Horizontal slices were prepared from Sprague–Dawley rats aged 18–25 days using slice preparation techniques as detailed in several prior publications from the Frazier lab (e.g. Lindsly and Frazier 2010). All experimental procedures were approved by the Institutional Animal Care and Use Committee of the University of Florida. The real time interface between the CA1 interneuron and the computer neuron was generated using the Real Time Experimental Interface (RTXI) and the dynamic clamp techniques described by Dorval et al. (2001). Custom modules for RTXI in C++ were written to generate model neuron (Wang Buzsaki (WB) neuron model for parvalbumin positive interneuron (Wang and Buzsáki 1996)) and to simulate the nonlinear threshold coupling synapse to create. In Fig. 1(c), we show the schematic wiring diagram for constructing a unidirectional hybrid network of WB neuron synaptically coupled to the CA1 interneuron. As can be seen from Figure 1C, the dc current bias required to the live CA1 neuron in the hybrid network intrinsically firing was generated in the ephys computer while the dynamic synaptic current was fed into the live neuron via the RTXI computer.

3 Effective connectivity estimation techniques

In this work, we consider four methods that are commonly employed to estimate EC in brain networks: GC, PDC, GPDC and PDM. Below we describe how these methods are applied to time series. The description includes the mathematical formulations of the measures and the determination of significance levels.

Let us begin by assuming that we have time series measurements from n neurons, which we represent in vector form as $\boldsymbol{X}(t) = [x_1(t), x_2(t), ..., x_n(t)]^T$. The goal is to estimate EC between these neurons i.e., determine whether neuron i with recorded time series $x_i(t)$ causally influences neuron j with recorded time series $x_j(t)$. Following Granger's original formulation (Granger 1980), three of the four EC measures considered here, GC, PDC, and GPDC, require $\boldsymbol{X}(t)$ to first be fit to an AR model.

For analysis of continuous valued time series data such as EEG or local field potentials, AR modeling is straightforward and has been applied in many previous instances. However, for nonlinear spiking neuronal data, which is typically represented in the form of point process binary time series data AR modeling is not directly applicable. The preferred approach in this case is to convert the point process data into a continuous valued time series data signal by using a low pass filter or a smoothing kernel (Baccala et al. 1998; Fanselow et al. 2001; Kaminski and Blinowska 1991). Other approach for the estimation of EC measures is to bypass the step of AR model fitting but rather obtain spectral representation of point process data and obtain estimates for EC in the frequency domain (Nedungadi et al. 2009). In our case, we have the continuous valued non-linear time series data derived from simulations of the ML neuron UCI network. Our goal is not to model the nonlinearity in the spikes per se but rather, the interactions between the coupled neuronal oscillators that is mediated through synapses and is reflected in the sub-threshold neuronal activity. We therefore chose to directly model the raw continuous valued time series data using an AR model of a very high order (Smirnov et al. 2007). Below we present a brief overview of AR model construction for neuronal oscillator datasets.

3.1 Autoregressive (AR) modeling

The vector autoregressive (VAR) model for $\boldsymbol{X}(t)$ has the following form (Lütkepohl 2010):

$$\boldsymbol{X}(t) = \sum_{k=1}^{p} \boldsymbol{A}_k \boldsymbol{X}(t-k) + \boldsymbol{\epsilon}(t) \tag{6}$$

$p \in \mathbb{I}$, is the VAR model order. The choice of p is usually set according to Akaike's information criterion (Akaike 1969), the Schwarz Bayesian information criterion (Schwarz 1978), or some other model order selection criterion (Brockwell and Davis 1991). The p coefficient matrices, $\boldsymbol{A}_k$, $(k = 1, \cdots, p)$, are each of dimension $n \times n$ and $\boldsymbol{\epsilon}(t)$, which represents the residual noise associated with the model, is a vector-valued white noise process with covariance matrix $\boldsymbol{\Sigma}$.

The coefficient matrices, $\boldsymbol{A}_k$ in Eq. (6), can be transformed to the frequency domain via Fourier transform (Box et al. 2008):

$$\boldsymbol{A}(f) = \boldsymbol{I} - \sum_{k=1}^{p} \boldsymbol{A}_k e^{-2\pi i f k} \tag{7}$$

The transfer matrix is defined as:

$$\boldsymbol{H}(f) = \boldsymbol{A}^{-1}(f) \tag{8}$$

where $\boldsymbol{A}(f)$ is defined in Eq. (7). The spectral matrix is defined through (Box et al. 2008):

$$\boldsymbol{S}(f) = \boldsymbol{H}(f)\boldsymbol{\Sigma}\boldsymbol{H}^{*}(f) \tag{9}$$

In this work, VAR model fitting was performed using the ARfit Matlab package (Schneider and Neumaier 2001) and the optimal model order of each time series was determined using Aikaike's final prediction error algorithm (Akaike 1969). Once a VAR model of $\boldsymbol{X}(t)$ is constructed, it is possible to apply the methods GC, PDC and GPDC to the data in order to obtain an estimate of EC.

3.2 Partial directed coherence

Here we review the mathematical formulation of both PDC and GPDC (Baccala and Sameshima 2001; Baccala et al. 2007). PDC from neuron j to neuron i is defined as (Baccala and Sameshima 2001):

$$\boldsymbol{PDC}_{j\to i}(f) = \frac{A_{ij}(f)}{\sqrt{\sum_{k=1}^{n} A_{kj}(f) A_{kj}^{*}(f)}} \tag{10}$$

where $\left|\boldsymbol{PDC}_{j\to i}(f)\right|$ represents the EC from neuron j to neuron i.

GPDC, a modified version of PDC, was introduced as a more robust measure of causality (Winterhalder et al. 2005; Baccala et al. 2007). GPDC incorporates values from the noise covariance matrix, $\boldsymbol{\Sigma}$, obtained when one fits the data, $\boldsymbol{X}(t)$, to a VAR model. These noise covariance values are used as weighting terms in the numerator and denominator of the original PDC measure giving the following equation for GPDC from neuron j to neuron i:

$$\boldsymbol{GPDC}_{j\to i}(f) = \frac{\frac{1}{\Sigma_{ii}} A_{ij}(f)}{\sqrt{\sum_{k=1}^{n} \frac{1}{\Sigma_{kk}^2} A_{kj}(f) A_{kj}^{*}(f)}} \tag{11}$$

where again, $\left|\boldsymbol{GPDC}_{j\to i}(f)\right|$ represents the EC from neuron j to neuron i.

3.3 Granger causality

While Granger's original formula for GC was a time domain measure, Geweke reformulated this measure in the frequency domain for the bivariate case (Geweke 1982). Geweke's measure, which we use in this work, requires both the transfer matrix, $\boldsymbol{H}(f)$, and the spectral matrix, $\boldsymbol{S}(f)$, defined in Eqs. (8) and (9).

For the case when $n = 2$, let us denote the two time series under consideration as $x_i(t)$ and $x_j(t)$. Then $\boldsymbol{S}(f)$, $\boldsymbol{H}(f)$, and $\boldsymbol{\Sigma}$ can be expanded as follows:

$$\boldsymbol{S}(f) = \begin{pmatrix} S_{ii}(f) & S_{ij}(f) \\ S_{ji}(f) & S_{jj}(f) \end{pmatrix}$$

$$\boldsymbol{H}(f) = \begin{pmatrix} H_{ii}(f) & H_{ij}(f) \\ H_{ji}(f) & H_{jj}(f) \end{pmatrix}$$

$$\boldsymbol{\Sigma} = \begin{pmatrix} \Sigma_{ii} & \Sigma_{ij} \\ \Sigma_{ji} & \Sigma_{jj} \end{pmatrix} \tag{12}$$

Then, according to Geweke, GC from $x_j(t)$ to $x_i(t)$ is defined as (Geweke 1982):

$$\boldsymbol{GC}_{j\to i}(f) = \ln \frac{S_{ii}(f)}{S_{ii}(f) - \left(\Sigma_{jj} - \Sigma_{ij}^2/\Sigma_{ii}\right) \mid H_{ij}(f) \mid^2} \tag{13}$$

The above formula is used to compute pairwise GC, that is, GC between two nodes. For a system with more than two nodes, however, this measure can give misleading results if it is simply applied repeatedly among pairs of nodes. An example of such a case involves three nodes, where one node drives the other two with differential time delays. Pairwise GC would indicate EC from the node that receives an earlier input to the node that receives a later input. Instead, a conditional GC measure should be applied in this case which estimates the EC between two nodes conditioned on a third node or set of nodes. For instance, if $n = 3$ with time series $x_i(t)$, $x_j(t)$, and $x_k(t)$, conditional GC computes the EC from $x_j(t)$ to $x_i(t)$ conditioned on $x_k(t)$. Geweke's frequency domain formulation has been extended to this conditional GC case as well (Geweke 1984; Ding et al. 2006). In this work, we use the partition matrix method introduced by Chen et al. for computing frequency-domain conditional GC in our 3-neuron networks (Chen et al. 2006).

3.4 Phase dynamics modeling

PDM was introduced by Rosenblum and Pikovsky specifically for detecting the directionality of coupling between coupled, narrow-band oscillators (Rosenblum

and Pikovsky 2001). Rather than utilizing the full time series signal, as in the case of GC and PDC, PDM deals only with time series of instantaneous phase, which we denote as $\phi(t)$.

Let $\phi_i(t)$ and $\phi_j(t)$ represent instantaneous phase for the two coupled oscillators i and j respectively. The phase increment $\phi_i(t+\tau) - \phi_i(t)$ at time step τ for oscillator i can be modeled by the following equation (Rosenblum and Pikovsky 2001):

$$\phi_i(t+\tau) - \phi_i(t) = F(\phi_i(t), \phi_j(t)) + \xi_i(t) \tag{14}$$

where ξ is zero mean white noise process and the function F is a trigonometric polynomial of the form

$$F(\phi_i(t), \phi_j(t)) = \sum_{m,n} \left[a_{m,n} \cos(m\phi_i(t) + n\phi_j(t)) + b_{m,n} \sin(m\phi_i(t) + n\phi_j(t)) \right] \tag{15}$$

The coefficients of Eq. (15), $a_{m,n}$ and $b_{m,n}$, are estimated using a least squares fit to the instantaneous phase time series. Following Rosenblum and Pikovsky (2001), we use third-order polynomials for Eq. (15).

The strength of the causal influence from oscillator j to oscillator i is determined by the steepness of the dependence of F on $\phi_j(t)$ i.e., $\partial F / \partial \phi_j(t)$. Thus, PDM from $j \to i$ is defined as:

$$\boldsymbol{PDM}_{j \to i} = \sqrt{\frac{1}{2\pi^2} \int_0^{2\pi} \int_0^{2\pi} \left(\frac{\partial F}{\partial \phi_j} \right)^2 d\phi_i d\phi_j} \tag{16}$$

3.5 Significance thresholds

In order to draw conclusions about the presence of EC in a network, the estimates of EC calculated via the methods described above must be compared to the null case. Here the null case consists of two independent nodes with no EC. By applying GC, PDC, GPDC and PDM to this null case, we can obtain, for each of these measures, significance thresholds above which EC is said to exist.

Surrogate testing was used to determine the significance thresholds for GC, PDC, GPDC and PDM. This was necessary in the case of spectral GC and GPDC since no analytical bounds have been derived for these measures. While analytical bounds do exist for PDC and PDM (Schelter et al. 2006), we chose to use surrogate testing for these measures as well in order to make the results more comparable to those obtained by GC and GPDC. In addition, there is some indication that numerical methods perform better on finite datasets than analytical bounds derived asymptotically (Davidson and MacKinnon 2003; MacKinnon 2006).

Significance levels were obtained by generating 5,000 surrogate time series, all of which exhibited no EC between their nodes. These surrogate time series were generated by first simulating the ML network in Section 2. Then the time series of each neuron was windowed into discrete blocks and these blocks were randomly shuffled in order to maintain the energy content of each signal while destroying the temporal relationship between signals (Kamiński et al. 2001). The EC measures were then applied to these surrogate datasets. Since GC, PDC and GPDC are a function of frequency, we considered only the maximum EC value across all frequencies (Chen et al. 2006; Blair and Karniski 1993). Finally, we used a p-value of $p = 0.05$ to calculate significance thresholds for each measure. If the EC value in Eq. (16) or the maximum EC over all frequencies in Eqs. (13), (10) and (11) is greater than the computed significance threshold, then a connection from $j \to i$ is said to exist.

4 Methods

We begin by defining the time series features used to characterize the datasets investigated in this study. These time series features were calculated using the voltage trace from the simulated ML network. In Fig. 2, we show an example of the raw voltage time trace and the estimated voltage time trace using an AR model of order $p = 200$, for the two unidirectionally coupled ML neurons.

4.1 Definition of time series features

We began by characterizing the time series according to 15 different statistical features. During the decision tree construction process, however, we found that three of these features: phase coherence, coefficient of variation and firing frequency, were overwhelmingly dominant and, by themselves, could be used to construct accurate decision trees. Interestingly, these features characterize the dynamical properties of the network, i.e., the level of synchrony and the noise in the network of coupled oscillators, which in previous works have been shown to play a significant role in affecting the performance of EC measures (Smirnov et al. 2007). These time series features are defined below.

1. Phase coherence (PC): is a measure of synchrony between two oscillators. Given two time series with

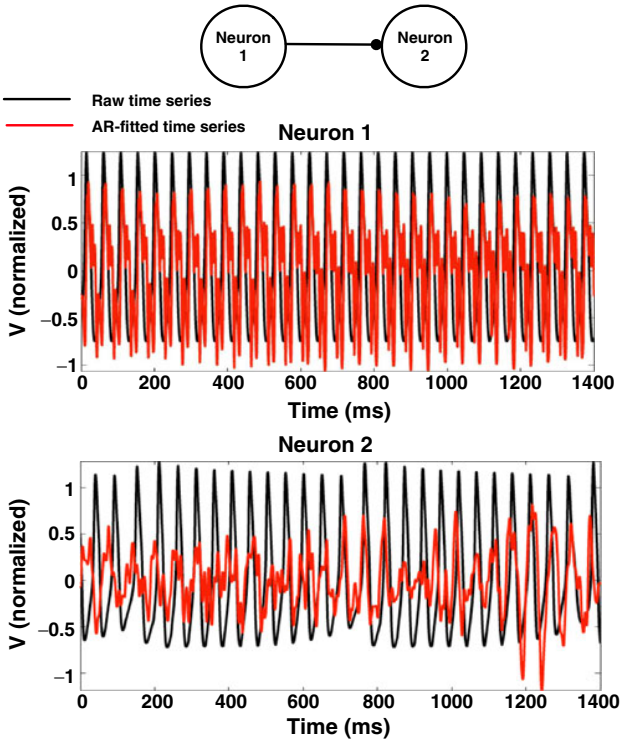

Fig. 2 Normalized membrane potential of two Morris–Lecar neurons coupled through nonlinear threshold coupling synapse. Traces in *black* show the raw time series generated from simulation of the ML network, while the traces in *red* show the corresponding time series data generated by fitting the raw time series data to an AR model with model order $p = 200$. In this example, the parameters of neuron 1 were set at $k = 0$, $D = 1$, and $I_{dc} = 80$ and the parameters of neuron 2 were set at $k = 0.5$, $D = 1$, and $I_{dc} = 50$

instantaneous phase, $\phi_i(t)$ and $\phi_j(t)$, PC can be defined as (Mormann et al. 2000):

$$\mathrm{PC}(i,\ j) = \sqrt{\langle \cos(\phi_i(t) - \phi_j(t))\rangle^2 + \langle \sin(\phi_i(t) - \phi_j(t))\rangle^2} \tag{17}$$

where $\langle\cdot\rangle$ denotes time averaging. This measure is symmetric in $\phi_i(t)$ and $\phi_j(t)$ and $\mathrm{PC}(i,\ j) = 1$ when there is complete phase synchrony between the oscillators, i.e., when $\phi_i(t) - \phi_j(t) = constant$.

2. Coefficient of variation of interspike interval (CV): is a measure of dynamical noise in the neuronal oscillator. Given neuronal membrane potential, one can estimate the inter-spike interval (ISI) as the time interval between consecutive crossings of the membrane potential with some threshold. From the distribution of ISIs we obtain the mean μ_{ISI} and the variance σ^2_{ISI}. CV is then obtained as (Perkel et al. 1967):

$$\mathrm{CV} = \frac{\sigma_{\mathrm{ISI}}}{\mu_{\mathrm{ISI}}} \tag{18}$$

A CV of one indicates a Poisson process where all spikes occur independently while a CV of zero indicates a series of perfectly periodic spikes. We introduce the following pair wise measure of CV to account for a given pair of neurons:

$$\mathrm{CV}_{\mathrm{mean}}(i,\ j) = \frac{1}{2}(\mathrm{CV}_i + \mathrm{CV}_j)$$
$$\mathrm{CV}_{\mathrm{diff}}(i,\ j) = \frac{1}{2}(\mathrm{CV}_i - \mathrm{CV}_j) \tag{19}$$

3. Firing frequency (FF): a measure of excitability of a neuronal oscillators, is obtained as

$$\mathrm{FF} = \frac{1}{\mu_{\mathrm{ISI}}} \tag{20}$$

We again introduce the following pair-wise measure for FF

$$\mathrm{FF}_{\mathrm{mean}}(i,\ j) = \frac{(\mathrm{FF}_i - \mathrm{FF}_j)}{\max(\mathrm{FF}_i, \mathrm{FF}_j)} \tag{21}$$

The time series features (given through Eqs. (17), (19) and (21)) can be calculated from the membrane voltage time series of a neuronal oscillator. This is in contrast to model parameters such as k, D, and I_{dc} which are often hidden in experimental datasets. Previous studies have focused either on finding regions of model parameter space where the methods for estimating EC fail (Winterhalder et al. 2007; Kayser et al. 2009; Lungarella et al. 2007), or on non-dynamical features of a dataset such as signal-to-noise ratio or dataset length that influence the accuracy of a given method for estimating EC (Astolfi et al. 2007; Smirnov and Andrzejak 2005). Unlike these past works, the current study presents results in the space of the time series features outlined above, making it more applicable for practitioners who wish to apply the data-driven methods considered here to estimate EC.

4.2 Decision tree construction

Here we present an overview of the procedure adopted to construct the decision tree using the time series features described in Section 4.1

1. Generate an ensemble of time series datasets by systematically varying the parameters, k, D, and I_{dc} of the ML neurons in Eq. (1) which are coupled according to Fig. 1(a). Repeat this for each of the three synapse types presented in Section 3.

2. Calculate the time series features defined in Section 4.1 for each dataset.
3. Estimate EC using GC, PDC, GPDC, and PDM for each time series.
4. Train a classifier for a given method for estimating EC by setting the time series features as predictors and the output generated by the chosen method as the response.
5. Test the classifiers by (a) generating experimental data sets using the dynamic clamp setup and (b) generating a new ensemble of 3-neuron time series datasets (Fig. 1(b)).

For step 1, a total of 1,000 time series datasets were generated for each synapse type by systematically varying the coupling strength k in the range [1e-4, 0.5] mS/cm^2, D of both neurons in the range [0, 80], and I_{dc} of both neurons in the range [40, 85] (Balenzuela and García-Ojalvo 2005). Only unidirectional couplings were considered. A total of $N = 51{,}000$ data points were generated for each time series. Time series features were calculated in step 2 as defined in Section 4.1. Instantaneous phase, which is needed to calculate phase coherence, was obtained via Hilbert transform of the voltage time series (Pikovsky et al. 2002). The four methods for estimating EC were applied to the datasets in step 3.

The classifiers in step 4 were constructed using Matlab's `classregtree` function which trains a decision tree based on a given set of *predictors* and *responses* (also referred to as *features* and *categories*, respectively) (Breiman et al. 1984). For each method and coupling type, a decision tree was constructed. In this work, the predictors are the time series features defined in Section 4.1 including PC(i, j), $\mathrm{CV}_{\mathrm{mean}}(i, j)$, abs($\mathrm{CV}_{\mathrm{diff}}(i, j)$), and abs($\mathrm{FF}_{\mathrm{diff}}(i, j)$) and the responses are the outputs generated by the four methods in step 3. Absolute values of $\mathrm{CV}_{\mathrm{diff}}(i, j)$ and $\mathrm{FF}_{\mathrm{diff}}(i, j)$ are used for the classifier since, in an experimental setting, there is no a priori ordering of neurons. Each time series dataset was treated as a separate instance and was used as input to construct the decision tree. For example, the GC/linear coupling decision tree was constructed by supplying the `classregtree` function with the PC(i, j), $\mathrm{CV}_{\mathrm{mean}}(i, j)$, abs($\mathrm{CV}_{\mathrm{diff}}(i, j)$), and abs($\mathrm{FF}_{\mathrm{diff}}(i, j)$) values of all 1,000 linear coupling datasets as predictors. In addition, the function was given the corresponding GC result as the response for each dataset. Responses were labeled as either '1' if GC detected the correct directionality of the interaction or '0' if GC failed to detect correct directionality. Similar decision trees were constructed for PDC, GPDC and PDM.

Decision trees were primarily used because they are amenable to easy interpretation, require little data preparation and have the ability to perform well with large amounts of data with short training time period. In addition, they had the lowest misclassification error compared to other classification methods such as linear or quadratic discriminant analysis, Naive Bayes, and support vector machines when applied to our datasets (see Table 1). The performance of the decision tree classifiers was verified using a ten-fold cross-validation scheme (Schaffer 1993). We note that no attempt was made to optimize the performance of any of the classifiers that we investigated for this study. Thus it is very likely that other classifiers such as support vector machines may very well have performance comparable to those obtained using the decision tree classifiers.

In step 5, we first address the issue of how reliable the decision tree classifiers are in predicting the performance of EC measures when applied to arbitrary network of coupled neuronal oscillators. We address this issue by generating experimental data from a hybird network comprising of a model neuron coupled to a living whole cell patch clamped neuron using the dynamic clamp setup.

We also tested the applicability of our decision tree classifiers to the general class of a multi-node neuronal network by first generating a new ensemble of 3-neuron time series datasets according to the network structure in Fig. 1(b). Values for the ML model parameters k, D, and I_{dc} were randomly selected within the aforementioned ranges and 1,000 new time series datasets were generated for each coupling type using the previously described methodology. The presence and directionally of the possible couplings in the network was set randomly. Next, we calculated a set of predictors from this new data that could be classified by our previously constructed decision trees. Once again, we used the time series features defined in Section 4.1 as predictors. In this case, time series features were calculated for each new test time series dataset by considering only

Table 1 Average test error of various classifiers trained on our datasets

Classifier type	Test error
Linear discriminant analysis	35.5%
Quadratic discriminant analysis	35.2%
Naive Bayes with kernel density estimation	26.0%
Support vector machine with third order polynomial kernel	26.6%
Decision tree	24.7%

Test error is averaged over the four EC measures and three coupling types

pairwise interactions. Thus, each time series dataset consisted of three values for each time series feature, i.e., PC(1, 2) captures the phase coherence between neuron 1 and neuron 2, PC(1, 3) the phase coherence between neuron 1 and 3, and PC(2, 3) the phase coherence between neuron 2 and 3, with the remaining time series features specified in a similar fashion. In this way, each dataset was decomposed into three separate predictors, one for each pairwise interaction in the network. For instance, given a single dataset, three predictors were constructed: one consisting of the PC(i, j), $\mathrm{CV}_{\mathrm{mean}}(i, j)$, $\mathrm{abs}(\mathrm{CV}_{\mathrm{diff}}(i, j))$, and $\mathrm{abs}(\mathrm{FF}_{\mathrm{diff}}(i, j))$ values between neurons 1 and 2, a second consisting of these time series features for neurons 1 and 3, and a third with these time series features for neurons 2 and 3. With an ensemble size of 1,000, a total of 3,000 predictors were constructed. The decision tree classifiers were then applied to this new set of test predictors, yielding a set of classifier responses. These classifier responses, labeled either '1' or '0', indicated whether a particular EC measure was predicted to be correct or incorrect by its corresponding decision tree.

Finally, we calculated the actual responses obtained when we applied each of the four methods, GC, PDC, GPDC and PDM, to the new 3-node network datasets. PDC and GPDC were applied as described in Eqs. (10) and (16) since these formulas implicitly handle networks with more than two nodes. Different formulas for GC and PDM, however, were needed in order to properly handle this multivariate data. A partition matrix method of computing conditional GC (Chen et al. 2006) was used for this purpose along with a general n-dimensional formula for PDM (Smirnov and Bezruchko 2009). The results of the four methods for estimating EC were labeled as either '1' or '0,' denoting that the method was either correct or incorrect, respectively. The classifier responses were then compared with the actual responses of a given EC measure in order to calculate the tree's accuracy.

The experimental procedure described above is illustrated in Fig. 3.

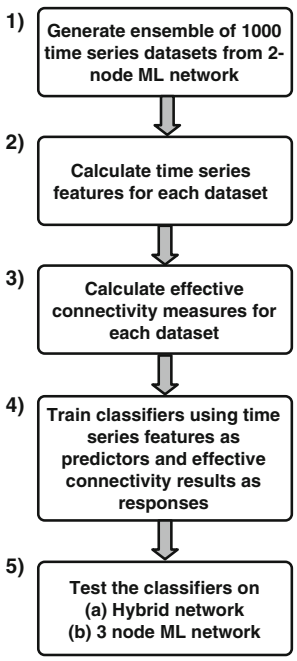

Fig. 3 Flowchart illustrating the experimental design of this study. Numbers correspond to the list in Section 4.2

5 Results

5.1 Decision trees

Decision trees were constructed for each of the four methods following the procedure described in Section 4.2. We also constructed classifiers based on linear and quadratic discriminant analysis, Naive Bayes, and support vector machines. We used ten-fold cross-validation on each of the resulting classifiers in order to estimate the test error, which is the expected misclassification error of a classifier when it is applied to data that is independent of the original training data (Schaffer 1993). Our results, presented in Table 1, show that the decision tree classifier had the lowest test error of the five classifiers we investigated.

After constructing our decision trees for each coupling type, it was found that the basic structure of the decision trees, such as the features on each branch and their ordering, was the same across all three types of coupling that we considered. However, the specific feature values on each decision branch point did vary among the different coupling types for each measure. An example of this is shown in Fig. 4 for GC.

Rather than present separate decision trees for each coupling type, we chose to average the feature values at these branch points in order to get a composite decision tree for each of the four methods that could be used regardless of the type of coupling between neuronal oscillators. Since a practitioner may not know the exact form of coupling between neurons in a given experimental dataset, this approach is also the most applicable in practice. The composite trees are shown in Fig. 5 and were used to derive the following results.

Each decision tree contains only a subset of the original four time series features used as predictors for generating the trees. This provides insight into the predictive features of a given dataset that are critical for each of the four methods in terms of their ability to correctly estimate EC in the network. The PDC tree is

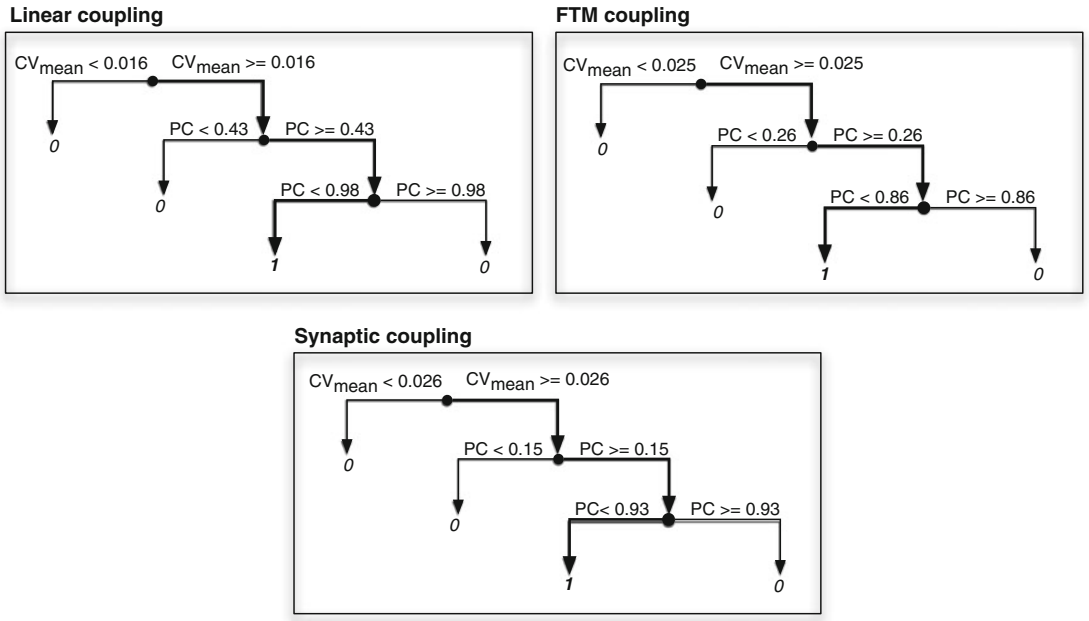

Fig. 4 Decision trees constructed for GC across three different coupling types considered. All trees share the same structure but vary in the exact predictor values at each decision point

the most extreme example as it only requires PC(i, j) to predict whether or not the method will work. The fact that PC is such a critical time series feature is a reflection of the importance of phase synchrony in determining EC via PDC. More specifically, as the degree of phase synchrony increases, PDC becomes less accurate as an EC measure. As further confirmation of PC's importance with respect to PDC, our results indicating that PDC is likely not to work when PC(i, j) $\geq$ 0.69 correspond to the results obtained in Smirnov et al.'s study which indicated that PC(i, j) values above 0.75 or, some cases, above 0.5, were detrimental to PDC (Smirnov et al. 2007).

The trees constructed for GC and GPDC are almost identical due to the fact that these methods nearly always predict the same EC for 2-node networks. For

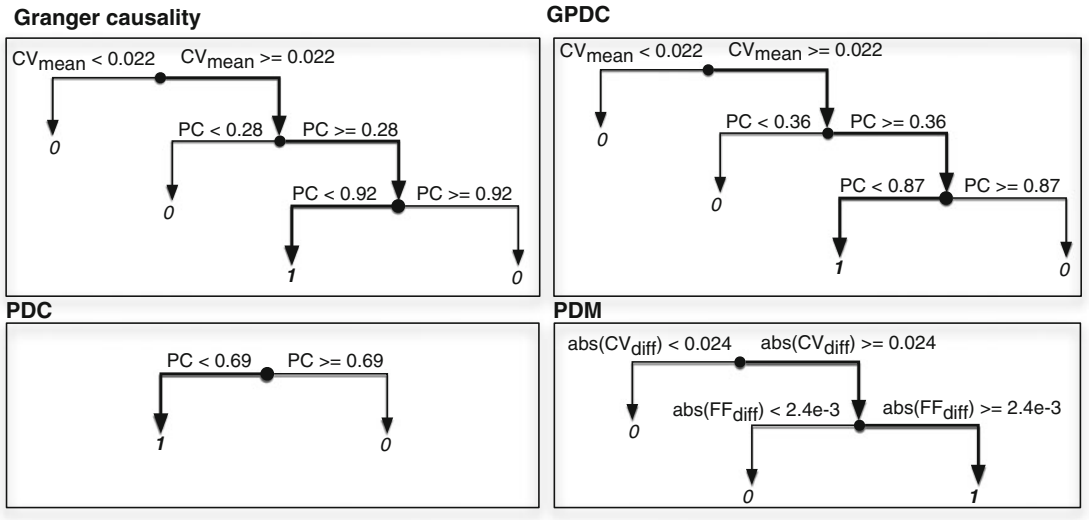

Fig. 5 Composite decision trees for all EC measures. These trees were constructed by averaging the predictor values at each decision point over all coupling types for each measure

instance, out of the 1,000, 2-node training datasets we considered, GC and GPDC agreed on the directionality of interaction 97.0%, 97.4%, and 97.8% of the time for linear, fast threshold modulation, and synaptic coupling, respectively. Thus, for both methods, the decision trees indicate that PC(i, j) and $CV_{mean}(i, j)$ are critical factors for determining correct EC. The fact that $CV_{mean}(i, j)$ must be equal or greater than 0.022 in the case of both GC and GPDC, is most likely a reflection of the fact that both methods require some amount of dynamical noise be present in the system in order for them to work. The requirement that PC(i, j) must be less than 0.92 or 0.87 for GC and GPDC, respectively, restricts the level of synchronization that can exist between two signals and is an expected requirement based on previous studies of these methods (Smirnov et al. 2007).

In contrast to the other methods considered, PDM is able, to some extent, to detect EC across different frequencies due to the m and n terms in Eq. (16) (Smirnov and Bezruchko 2009). In fact, variation in the intrinsic firing frequencies between neuronal oscillators is beneficial to the method because it results in a $\phi_1(t)$ versus $\phi_2(t)$ trajectory that fills up the phase space (Rosenblum and Pikovsky 2001). Only in this case can the function F in Eq. (16) be properly estimated with $\phi_i(t)$ and $\phi_j(t)$ as independent variables. This is illustrated in Fig. 6 where the $\phi_1(t)$ versus $\phi_2(t)$ phase space trajectories for two datasets, one with a high abs($FF_{diff}(i, j)$) and one with a low abs($FF_{diff}(i, j)$), are shown. Despite previous observations that PDM accuracy is highly dependent on PC(i, j) (Smirnov et al. 2007), our results indicate that PC(i, j) is not as critical a factor in determining whether the method will fail as other metrics such as $FF_{diff}(i, j)$ and $CV_{mean}(i, j)$.

We calculated the sensitivity and specificity of each decision tree as follows:

$$\text{sensitivity} = \frac{\#\text{ of true positives}}{\#\text{ of true positives} + \#\text{ of false negatives}} \tag{22}$$

$$\text{specificity} = \frac{\#\text{ of true negatives}}{\#\text{ of true negatives} + \#\text{ of false positives}} \tag{23}$$

where true positives in this case occur when the decision tree labels a dataset as '1' and the EC measure produces correct results, true negatives occur when the decision tree labels a dataset as '0' and the EC measure produces incorrect results, false positives occur when the decision tree labels a dataset as '1' and the given method for estimating EC produces incorrect results, and false negatives occur when the decision tree labels a dataset as '0' and the given method produces correct results. A sensitivity of 100% means the decision tree identifies all cases when the method is correct and a specificity of 100% means the decision tree identifies all cases when the method produces incorrect results. Composite trees for each method were used along with ten-fold cross-validation to calculate sensitivity and specificity values. The results are presented in Table 2.

In light of these results, we can now comment on our choice of using only unidirectional coupling in our

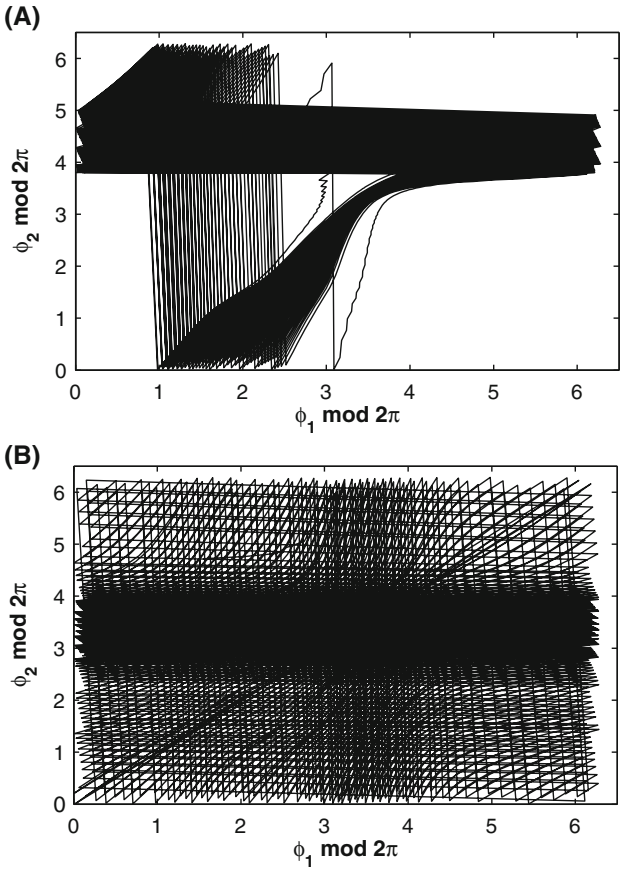

Fig. 6 The trajectory of two instantaneous phases, $\phi_1(t)$ versus $\phi_2(t)$, from datasets with linear coupling and (**a**) abs($FF(i, j)_{diff}$) = 2.4e-4, (**b**) abs($FF_{diff}(i, j)$) = 0.4. A larger abs($FF_{diff}(i, j)$) value results in the trajectory filling up more of the phase space

Table 2 Decision tree sensitivity and specificity values

	Sensitivity	Specificity
GC Tree	72.0 (±7.7)%	81.7 (±3.1)%
GPDC Tree	74.5 (±7.9)%	81.5 (±3.0)%
PDC Tree	66.4 (±4.5)%	81.7 (±3.9)%
PDM Tree	80.5 (±4.4)%	77 (±3.3)%

95% confidence intervals are given in parentheses

ensemble of training data. When we included time series datasets with bidirectional coupling in our training ensemble, the sensitivity of the decision trees dropped significantly. However, when we applied our decision trees that were based only on unidirectional coupling to datasets with bidirectional coupling, the sensitivity was not affected. This indicates that the space of time series features where unidirectional coupling can be detected is much more restrictive than those regions where bidirectional coupling can be detected. The reason for this is that bidirectional coupling biases the decision trees toward high values of phase coherence since, regardless of actual coupling directionality, a high phase coherence value almost always results in the EC measures predicting bidirectional coupling between neurons. Thus, if we included bidirectional connections in our training data, the decision trees would favor datasets with a high phase coherence value even though this is generally detrimental for detecting unidirectional coupling. As a result we decided to use only unidirectionally coupled ML network datasets to construct our classifiers.

Since this analysis was performed on a simulated networks of 2 nodes, the question remains as to the general applicability of decision trees for real biological networks as well as for analyzing EC measure applicability in larger networks. We address these issues in the next two sections.

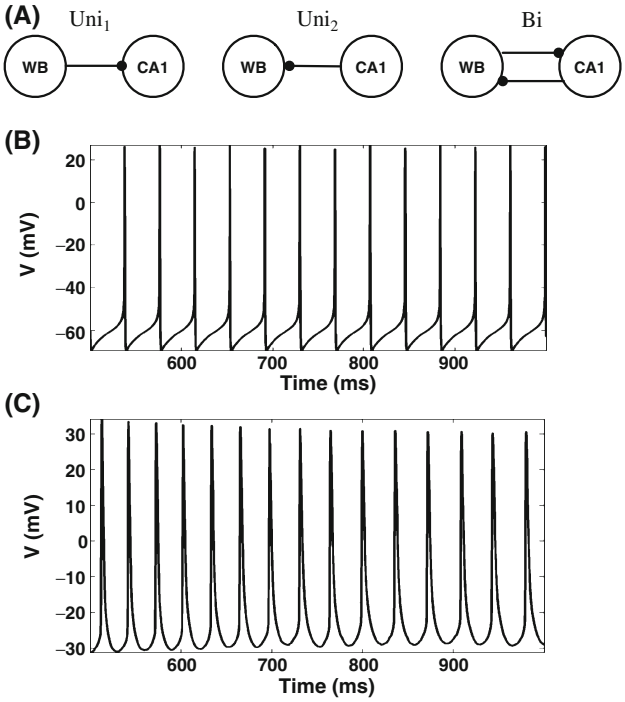

Fig. 7 (**a**) Schematic of the network configuration of the hybrid network constructed using dynamic clamp set up. (**b**) Raw voltage trace of the Wang Buzsaki interneuron model. (**c**) Raw voltage trace of the whole cell patched CA1 stratum orien interneuron

5.2 Decision tree performance on experimental datasets

As explained in Section 5.1, the decision trees were derived using simulated time series data generated from a network of unidirectionally coupled ML neurons. In this section, we ask how reliable these decision trees are in predicting the performance of a given method to estimate EC on real biological neuronal networks. In order to test the general applicability of these decision trees, we used the dynamic clamp set-up to generate hybrid experimental datasets comprised of a model Wang Buzsaki (WB) interneuron (Wang and Buzsáki 1996) (intrinsically firing at 26 Hz) coupled to an interneuron in the CA1 stratum orien (receiving a constant DC bias current such that the neuron is intrinsically firing at mean firing rate of 33 Hz) via a nonlinear threshold coupling synapse model. In Fig. 7(a), we show the three network configurations in which the model WB neuron was coupled to the CA1 interneuron. In Fig. 7(b) and (c), we show the raw time trace for baseline firing activity of the two coupled neurons respectively. For each network configuration, the coupling strength was varied between 0.02 mS/cm^2 and 0.07 mS/cm^2 to generate a total of 21 datasets. The predicted decision tree results as well as the actual EC measure results are shown in Table 3. For each of the four EC measures, the column labeled as predicted refers to the EC value reported by the decision tree for a given classifier, while the column labeled actual refers to the estimated EC found by applying each of the four methods for estimating EC. We see that all the decision trees are quite robust in that the decision tree classifier correctly predicts (TP+TN) the performance of each of the four EC measures >80% of the time. These results support the claim that the decision trees derived from simulated time series data generated by a relatively simple network of two unidirectionally coupled ML neurons can be generically applied to any arbitrary pair of oscillatory neuronal datasets.

5.3 Extension to larger networks

We applied the classifier decision trees of Fig. 5 to time series datasets generated from an ensemble of 3-neuron networks. A given dataset from this ensemble was classified a total of three times by the decision tree, once for each of its three pairwise interactions, with

Table 3 Performance of decision tree classifiers on experimental data sets

Network	Coupling (mS/cm^2)	Features $\{\|CV_{diff}\|, CV_{mean}, \|FF_{diff}\|, PC\}$	PDC pred, act	GPDC pred, act	GC pred, act	PDM pred, act
Baseline	No connection	{0.156, 0.098, 0.198, 0.607}	0, 0	1, 1	1, 1	1, 1
Bi	0.02	{0.044, 0.164, 0.208, 0.840}	0, 0	0, 1	1, 1	1, 1
Uni_1	0.02	{0.153, 0.135, 0.396, 0.851}	0, 0	1, 1	1, 1	1, 1
Uni_2	0.02	{0.103, 0.110, 0.258, 0.63}	1, 1	1, 1	1, 1	1, 1
Bi	0.0225	{0.063, 0.148, 0.061, 0.841}	0, 0	1, 1	1, 0	1, 1
Uni_1	0.0225	{0.146, 0.132, 0.286, 0.842}	0, 0	1, 1	1, 1	1, 1
Uni_2	0.0225	{0.121, 0.119, 0.043, 0.681}	1, 1	1, 1	1, 1	1, 1
Bi	0.025	{0.094, 0.016, 0.080, 0.743}	0, 0	0, 0	0, 0	1, 1
Uni_1	0.025	{0.111, 0.021, 0.001, 0.842}	0, 0	0, 0	0, 0	0, 0
Uni_2	0.025	{0.150, 0.016, 0.002, 0.839}	0, 1	0, 1	0, 1	0, 0
Bi	0.03	{0.007, 0.152, 0.077, 0.846}	0, 1	1, 1	1, 1	0, 0
Uni_1	0.03	{0.043, 0.136, 0.001, 0.862}	0, 0	1, 1	1, 1	0, 0
Uni_2	0.03	{0.120, 0.122, 0.092, 0.758}	0, 0	1, 1	1, 1	1, 0
Bi	0.0325	{0.078, 0.122, 0.046, 0.849}	0, 0	1, 1	1, 0	1, 1
Uni_1	0.0325	{0.105, 0.111, 0.267, 0.842}	0, 1	1, 1	1, 1	1, 1
Uni_2	0.0325	{0.049, 0.212, 0.539, 0.617}	1, 1	1, 1	1, 1	1, 0
Bi	0.035	{0.128, 0.123, 0.0241, 0.669}	1, 1	1, 1	1, 1	1, 1
Uni_1	0.035	{0.136, 0.127, 0.256, 0.843}	0, 1	1, 1	1, 1	1, 0
Uni_2	0.035	{0.055, 0.161, 0.121, 0.767}	0, 0	1, 1	1, 0	1, 1
Bi	0.07	{0.056, 0.128, 0.039, 0.815}	0, 0	1, 1	1, 1	1, 1
Uni_1	0.07	{0.145, 0.131, 0.266, 0.827}	0, 1	1, 1	1, 1	1, 0
Uni_2	0.07	{0.044, 0.170, 0.092, 0.783}	0, 0	1, 0	1, 1,	1, 1
Statistics			TP = 4; TN = 13 FP = 0; FN = 5	TP = 17; TN = 2 FP = 1; FN = 2	TP = 16; TN = 2 FP = 3; FN = 1	TP = 14; TN = 4 FP = 4; FN = 0

pred: EC estimated from the decision tree classifier; *act*: EC directly estimated by applying the method; *0* implies incorrectly estimated EC; *1* implies correctly estimated EC

the following results: a dataset could either have all of its pairwise interactions classified as '1', two pairwise interactions classified as '1' and one as '0', one pairwise interaction classified as '1' and two as '0', or all three classified as '0.'

Multivariate EC measures were applied to each dataset. We then calculated the likelihood that a given EC measure correctly identified the directionality of all interactions in the 3-neuron network given the number of pairwise network interactions classified as '1' by the decision tree. For example, consider a 3-neuron network with coupling from neuron 1 to 2 and from neuron 3 to 1. Given that only two of the three pairwise interactions in this network were classified by the decision as '1', we calculate the likelihood that an EC measure will correctly identify the correct network coupling from neuron 1 to 2 and 3 to 1. These likelihoods are presented in Table 4. Composite trees for each method were used for classification.

In order for all of the four methods considered here to be correct with probability greater than 50%, a majority of the pairwise interactions in the network must be classified by the decision tree as '1.' This result is shown in the third column of Table 4 which gives the accuracy of each EC measure given that two of the three pairwise interactions are '1.' These results are not significantly different from the sensitivity values in Table 2. On the other hand, accuracy percentages for the EC measures when all three pairwise interactions are classified as '0' in a 3-node network are presented in the first column of Table 4. In this case, the probability of any given method succeeding is less than 20%. For instance, the probability that GC gives correct results in this case is only $16 \pm 6.6\%$. Given these accuracies in the first column of Table 4, none of these measures should be applied if all pairwise interactions in a dataset

Table 4 Likelihood that a given EC measure correctly identifies directionality in the network given the number of pairwise interactions classified as '1'

	0 out of 3 '1'	1 out of 3 '1'	2 out of 3 '1'
GC	12 (±3.3)%	20 (±3.5)%	67 (±7.0)%
GPDC	12 (±4.4)%	43 (±4.6)%	66 (±8.3)%
PDC	16 (±6.6)%	46 (±4.0)%	74 (±3.9)%
PDM	18 (±5.7)%	25 (±2.4)%	84 (±5.4)%

95% confidence intervals are given in parentheses

are categorized as '0' by the decision tree since, with high probability, the results will in fact be incorrect.

6 Discussion

Numerous studies have applied linear methods such as GC and PDC or nonlinear methods such as PDM to neural datasets in an attempt to gain insight into the directionality of interactions in the brain (Brovelli et al. 2004; Cadotte et al. 2010; Liao et al. 2010; Chen et al. 2006; Havlicek et al. 2010; Sato et al. 2009). Datasets are generally considered amenable to such an analysis as long as they are stationary. The results of this study demonstrate the necessity for analyzing time series datasets beyond just determining their stationarity.

Synchrony is one example of a time series feature that can result in the failure of many methods for the right estimating EC, and previous work has indicated approximate bounds on the degree of phase coherence between two oscillators above which several of these methods tend to fail (Smirnov et al. 2007; Bezruchko et al. 2003). We extended these results by refining the limits on phase coherence as well as considering limits on other time series features, such as noise and firing frequency, for three of the most widely used linear methods for estimating EC, GC, PDC and GPDC, as well as PDM, which can handle some nonlinearities. This is the first systematic comparative study of these four methods as they apply to narrow-band oscillatory data.

In addition, we considered several realistic models for neuronal synapses. The observed consistency in the derived decision trees regardless of coupling type demonstrates that our findings can be applied to time series datasets even when the coupling type is unknown. Importantly, the features we considered are observable from the time series of the oscillators themselves which means that practitioners can readily apply our results to their experimental datasets. This is in contrast to studies which investigate the applicability of EC measures in terms of model parameters, such as coupling strength, which are not as evident from a time series alone (Winterhalder et al. 2007; Kayser et al. 2009; Lungarella et al. 2007).

Our overall goal is to develop a methodology based on the use of decision tree classifiers to assess whether a given TSI technique for estimating EC will produce correct results when applied to a given dataset based on the observable, dynamical characteristics of the datasets. In this work, we primarily focused on the development of our proposed methodology based on decision tree classifiers to access EC in a network of two coupled neuronal oscillators. The decision tree classifiers were trained and tested using simulated time series data generated from a two node network of unidirectionally coupled ML neuron models. We note that the structure of the decision trees may very well depend on the dynamical properties and the bifurcation mechanism for spike generation of the neuron model used to generate the network time series data. As stated earlier, our primary purpose in this work was to propose a new framework based on the application of decision tree classifiers aimed towards ultimately addressing the general question of characterizing the circumstances under which TSI techniques will produce correct inferences. Systematic study of the decision tree structure dependence on the neuron and the network type remains a topic of future investigation. Rather, here we focus on simple experimental demonstration for the reliability of the two node-decision tree classifiers a hybrid network of a model neuron (WB interneuron model) coupled to a live neuron using dynamic clamp set up.

Furthermore, we studied the applicability of the two-node decision tree classifiers for analyzing the performance of TSI techniques when applied to networks with greater than two nodes. Specifically we consider a 3 node network and empirically demonstrate that the likelihood of a given TSI technique to correctly estimate EC in the network is very low if the two node decision tree fails to identify any of the three pairwise interactions in the network. As such, we note that the pairwise time series features extracted from multivariate dataset may not include useful information to allow for distinguishing the direct causal interactions from indirect ones. However, this does not preclude the possibility that one can identify rules, which when applied to such computed features can allow one to distinguish the regions where TSI technique produces correct EC results from the region where they fail to do so. We note that in this work we have not demonstrated that this can be done for a general class of networks with more than three nodes. The detailed study of this problem is beyond the scope present investigation and is a topic of current active research within our group.

Based on our analysis of the three node network, we make some practical suggestions for the utility of the two-node decision tree classifiers when assessing performance of a given TSI technique in estimating EC in multivariate neuronal datasets. Our results from 3-node networks strongly suggests that if all pairwise interactions are classified as '0' by the decision tree of a given method, then the method should not be applied to the data since we expect the results to be incorrect. Based on this observation, we suggest that the practitioners first use the two-node decision trees

derived in this work to determine a classification for each of the pairwise interactions in their network. If a majority (>50%) of these interactions are classified as '0' by decision tree for given method, the method should not be applied since the results will most likely be incorrect. If a majority are classified as '1', on the other hand, the method can be applied with an expected probability of success greater than 66%. In addition, our results from 3-node networks strongly suggests that for any network, regardless of size, if all pairwise interactions are classified as '0' by the decision tree of a given method, then the method should not be applied to the data since we expect the results to be incorrect.

In summary, following key conclusions can be made from present work:

- The decision trees presented in this work provide a methodology for determining the applicability of a given method to estimate EC from a given set of time series data.
- This decision tree methodology can be applied without any prior knowledge of network structure or dynamics since all the time series features used to determine applicability can be measured directly from the time series themselves.
- In the case of small, 2–3 node networks, our results can be applied directly.
- For larger networks, we recommend that a given method not be applied if a majority of its pairwise interactions are classified as incorrect by the decision tree of that method.
- In contrast to GC, PDC and GPDC, differences in intrinsic firing frequencies between two time series is beneficial for PDM since it results in a more dispersed instantaneous phase trajectory.

We conclude by noting that our results and the conclusions summarized above represent the first steps in our efforts to develop a general quantitative framework to address the key question: Which TSI techniques will perform well in order to extract EC information from a given multivariate neuronal time series data?

As we make further progress, some of the specific questions of future research interest for us are:

- Characterize the dependence of decision tree classifiers based on the dynamic structure of the underlying neuronal models
- Extend the proposed framework of decision tree classifiers to tackle large neuronal networks (greater than 3 node)
- Extend the proposed framework to analyze connectivity amongst multivariate EEG time series data.

Acknowledgements This work was partially funded from the start-up funding to SST through the Dept of Pediatrics at UF and the startup funding to WOO and alumina fellowship to ERB through the Dept of Biomedical Eng at UF. SST and PRC were partially funded through the Children's Miracle Network Funds and Eve and B. Wilder Center of Excellence for Epilepsy Research. PPK was partially funded through the Eckis Professor Endowment at the University of Florida. We appreciate constructive feedback from Dr. Alex Cadotte. We also acknowledge the generosity of Dr CJ Frazier for allowing access to his electrophysiology rig set up and Ms. Aishwarya Parthasarthy for assistance in setting up the dynamic clamp and collection of experimental datasets. We finally acknowledge assistance from Mr. Kyungpyo Hong in generating Fig. 2 of the manuscript.

References

Abarbanel, H., Gibb, L., Huerta, R., & Rabinovich, M. (2003). Biophysical model of synaptic plasticity dynamics. *Biological Cybernetics, 89*, 214.

Akaike, H. (1969). Fitting autoregressive models for prediction. *Annals of the institute of Statistical Mathematics, 21*, 243.

Astolfi, L., Cincotti, F., Mattia, D., Marciani, M., Baccala, L., Fallani, F., et al. (2007). Comparison of different cortical connectivity estimators for high-resolution eeg recordings. *Human Brain Mapping, 28*, 143.

Baccala, L., & Sameshima, K. (2001). Partial directed coherence: a new concept in neural structure determination. *Biological Cybernetics, 84*(6), 463–474.

Baccala, L., Sameshima, K., Ballester, G., Valle, A. D., & Timo-Iaria, C. (1998). Studying the interaction between brain structures via directed coherence and granger causality. *Applied Signal Processing, 5*(1), 40.

Baccala, L., Sameshima, K., & Takahashi, D. (2007). Generalized partial directed coherence. In *Proceedings of the 15th international conference on digital signal processing, Cardiff, Wales, UK* (pp. 163–166).

Balenzuela, P., & García-Ojalvo, J. (2005). Role of chemical synapses in coupled neurons with noise. *Physical Review. E, Statistical, Nonlinear and Soft Matter Physics, 72*(2 Pt 1), 021901.

Bennett, M. (1997). Gap junctions as electrical synapses. *Journal of Neurocytology, 26*, 249.

Bezruchko, B., Ponomarenko, V., Rosenblum, M., & Pikovsky, A. (2003). Characterizing direction of coupling from experimental observations. *Chaos: An Interdisciplinary Journal of Nonlinear Science, 13*, 179.

Blair, R., & Karniski, W. (1993). An alternative method for significance testing of waveform difference potentials. *Psychophysiology, 30*, 518.

Box, G., Jenkins, G., & Reinsel, G. (2008). *Time series analysis: Forecasting and control* (4th ed.). Hoboken: Wiley.

Breiman, L., Friedman, J., Stone, C., & Olshen, R. (1984). *Classification and regression trees*. New York: Chapman and Hall.

Brockwell, P., & Davis, R. (1991). *Time series: Theory and methods*. New York: Springer.

Brovelli, A., Ding, M., Ledberg, A., Chen, Y., Nakamura, R., & Bressler, S. (2004). Beta oscillations in a large-scale sensorimotor cortical network: Directional influences revealed by granger causality. *Proceedings of the National Academy of Sciences of the United States of America, 101*(26), 9849–9854.

Buzsaki, G. (2006). *Rhythms of the brain*. Oxford: Oxford University Press.

Buzsaki, G., & Draguhn, A. (2004). Neuronal oscillations in cortical networks. *Science, 304*(5679), 1926–1929.

Cadotte, A., DeMarse, T., Mareci, T., Parekh, M., Talathi, S., Hwang, D. U., et al. (2010). Granger causality relationships between local field potentials in an animal model of temporal lobe epilepsy. *Journal of Neuroscience Methods, 189*, 121–129.

Chen, Y., Bressler, S., & Ding, M. (2006). Frequency decomposition of conditional granger causality and application to multivariate neural field potential data. *Journal of Neuroscience Methods, 150*(2), 228.

Chow, C., & Kopell, N. (2000). Dynamics of spiking neurons with electrical coupling. *Neural Computation, 12*(7), 1643.

Davidson, R., & MacKinnon, J. (2003). *Econometric theory and methods*. Oxford: Oxford University Press.

Deister, C., Teagarden, M., Wilson, C., & Paladini, C. (2009). An intrinsic neuronal oscillator underlies dopaminergic neuron bursting. *Journal of Neuroscience, 29*, 15888–15897.

Ding, M., Chen, Y., & Bressler, S. (2006). Granger causality: basic theory and application to neuroscience. In B. Schelter, M. Winterhalder, & J. Timmer (Eds.), *Handbook of time series analysis* (p. 451). Weinheim: Wiley-VCH.

Dorval, A. D., Christini, D. J., & White, J. A. (2001). Real-time linux dynamic clamp: A fast and flexible way to construct virtual ion channels in living cells. *Annals of Biomedical Engineering, 29*(10), 897–907.

Ermentrout, B. (1996). Type 1 membranes, phase resetting curves, and synchrony. *Neural Computation, 8*(5), 979–1001.

Fanselow, E. E., Sameshima, K., Baccala, L. A., & Nicolelis, M. A. (2001). Thalamic bursting in rats during different awake behavioral states. *Proceedings of the National Academy of Sciences of the United States of America, 98*(26), 15330–15335. doi:10.1073/pnas.261273898.

Fries, P. (2009). Neuronal gamma-band synchronization as a fundamental process in cortical computation. *Annual Review of Neuroscience, 32*, 209–224.

Friston, K. (2002). Functional integration and inference in the brain. *Progress in Neurobiology, 68*(2), 113–143.

Geweke, J. (1982). Measurement of linear dependence and feedback between multiple time series. *Journal of the American Statistical Association, 77*(378), 304.

Geweke, J. (1984). Measures of conditional linear dependence and feedback between time series. *Journal of the American Statistical Association, 79*(388), 907–915.

Granger, C. (1969). Investigating causal relations by econometric models and cross-spectral methods. *Econometrica: Journal of the Econometric Society, 37*(3), 424.

Granger, C. (1980). Testing for causality: A personal viewpoint. *Journal of Economic Dynamics & Control, 2*, 329–352.

Hammond, C., Bergman, H., & Brown, P. (2007). Pathological synchronization in Parkinson's disease: networks, models and treatments. *Trends in Neuroscience, 30*(7), 357–364.

Havlicek, M., Jan, J., Brazdil, M., & Calhoun, V. (2010). Dynamic granger causality based on kalman filter for evaluation of functional network connectivity in FMRI data. *NeuroImage, 53*, 65–77.

Izhikevich, E. (2007). *Dynamical systems in neuroscience: The geometry of excitability and bursting*. Cambridge: MIT Press.

Kaminski, M., & Blinowska, K. (1991). A new method of the description of the information flow in the brain structures. *Biological Cybernetics, 65*, 203–210.

Kamiński, M., Ding, M., Truccolo, W., & Bressler, S. (2001). Evaluating causal relations in neural systems: Granger causality, directed transfer function and statistical assessment of significance. *Biological Cybernetics, 85*(2), 145.

Kayser, A., Sun, F., & D'Esposito, M. (2009). A comparison of granger causality and coherency in FMRI-based analysis of the motor system. *Human Brain Mapping, 30*(11), 3475.

Lecar, H. (2007). Morris–lecar model. *Scholarpedia, 2*, 1333. www.scholarpedia.com.

Liao, W., Mantini, D., Zhang, Z., Pan, Z., Ding, J., Gong, Q., et al. (2010). Evaluating the effective connectivity of resting state networks using conditional granger causality. *Biological Cybernetics, 102*(1), 57–69.

Lindsly, C., & Frazier, C. J. (2010). Two distinct and activity-dependent mechanisms contribute to autoreceptor-mediated inhibition of gabaergic afferents to hilar mossy cells. *Journal of Physiology, 588*(Pt 15), 2801–22. doi:10.1113/jphysiol.2009.184648.

Lungarella, M., Ishiguro, K., Kuniyoshi, Y., & Otsu, N. (2007). Methods for quantifying the causal structure of bivariate time series. *International Journal of Bifurcation and Chaos, 17*, 903–921.

Lütkepohl, H. (2010). *New introduction to multiple time series analysis*. New York: Springer.

MacKinnon, J. (2006), Bootstrap methods in econometrics. *Economic Record, 82*, S2.

Mormann, F., Lehnertz, K., David, P., & Elger, C. (2000). Mean phase coherence as a measure for phase synchronization and its application to the eeg of epilepsy patients. *Physica D: Nonlinear Phenomena, 144*, 358.

Morris, C., & Lecar, H. (1981). Voltage oscillations in the barnacle giant muscle fiber. *Biophysical Journal, 35*(1), 193–213.

Nedungadi, A. G., Rangarajan, G., Jain, N., & Ding, M. (2009). Analyzing multiple spike trains with nonparametric granger causality. *Journal of Computational Neuroscience, 27*(1), 55–64. doi:10.1007/s10827-008-0126-2.

Perkel, D., Gerstein, G., & Moore, G. (1967). Neuronal spike trains and stochastic point processes: I. the single spike train. *Biophysical Journal, 7*(4), 391–418.

Pikovsky, A., Rosenblum, M., & Kurths, J. (2002). *Synchronization: A universal concept in nonlinear sciences*. Cambridge: Cambridge University Press.

Rosenblum, M., & Pikovsky, A. (2001). Detecting direction of coupling in interacting oscillators. *Physical Review E, 64*(4), 45202.

Sato, J., Takahashi, D., Arcuri, S., Sameshima, K., Morettin, P., & Baccalá, L. (2009). Frequency domain connectivity identification: An application of partial directed coherence in FMRI. *Human Brain Mapping, 30*(2), 452.

Schaffer, C. (1993). Selecting a classification method by cross-validation. *Machine Learning, 13*, 135–143.

Schelter, B., Winterhalder, M., Eichler, M., Peifer, M., Hellwig, B., Guschlbauer, B., et al. (2006). Testing for directed influences among neural signals using partial directed coherence. *Journal of Neuroscience Methods, 152*(1–2), 210–219.

Schneider, T., & Neumaier, A. (2001). Algorithm 808: Arfit—a matlab package for estimation and spectral decomposition of multivariate autoregressive models. *ACM Transactions on Mathematical Software, 27*, 58–65.

Schwarz, G. (1978). Estimating the dimension of a model. *Annals of Statistics, 6*, 461–464.

Smirnov, D., & Andrzejak, R. (2005). Detection of weak directional coupling: Phase-dynamics approach versus state-space approach. *Physical Review E, 71*(3), 36207.

Smirnov, D., & Bezruchko, B. (2009). Detection of couplings in ensembles of stochastic oscillators. *Physical Review E, 79*(4), 046204.

Smirnov, D., Schelter, B., Winterhalder, M., & Timmer, J. (2007). Revealing direction of coupling between neuronal oscillators from time series: Phase dynamics modeling versus partial directed coherence. *Chaos: An Interdisciplinary Journal of Nonlinear Science, 17*, 013111.

Somers, D., & Kopell, N. (1993). Rapid synchronization through fast threshold modulation. *Biological Cybernetics, 68*, 393.

Sporns, O. (2010). *Networks of the brain*. Cambridge: MIT Press.

Talathi, S., Hwang, D. U., Carney, P., & Ditto, W. (2010). Synchrony with shunting inhibition in a feedforward inhibitory network. *Journal of Computational Neuroscience, 28*, 305.

Uhlhaas, P., & Singer, W. (2010). Abnormal neural oscillations and synchrony in schizophrenia. *Nature Reviews. Neuroscience, 11*, 100–113.

Wang, X. J., & Buzsáki, G. (1996). Gamma oscillation by synaptic inhibition in a hippocampal interneuronal network model. *Journal of Neuroscience, 16*(20), 6402–6413.

Ward, L. (2003). Synchronous neural oscillations and cognitive processes. *Trends in Cognitive Science, 7*(12), 553–559.

Winterhalder, M., Schelter, B., Hesse, W., Schwab, K., Leistritz, L., Klan, D., et al. (2005). Comparison of linear signal process techniques to infer directed interactions in multivariate neural systems. *Signal Processing, 85*(11), 2137–2160.

Winterhalder, M., Schelter, B., & Timmer, J. (2007). Detecting coupling directions in multivariate oscillatory systems. *International Journal of Bifurcation and Chaos, 17*, 3725–3739.